Journal of Alloys and Compounds 509 (2011) 6296–6301

Contents lists available at ScienceDirect

Journal of Alloys and Compounds

journal homepage: www.elsevier.com/locate/jallcom

Effects of equal channel angular extrusion and aging treatment on R phase transformation behaviors and Ti_3Ni_4 precipitates of Ni-rich TiNi alloys

Xiaoning Zhang[a], Baoyu Xia[b,c], Jie Song[a], Bin Chen[d], Xiaolin Tian[d], Yingmin Hao[d], Chaoying Xie[a,*]

[a] State Key Lab. of Metal Matrix Composites, School of Materials Science and Engineering, Shanghai Jiao Tong University, Shanghai 200240, China
[b] Energy Research Institute, Nanyang Technological University, 70 Nanyang Drive 637457, Singapore
[c] School of Chemical and Biomedical Engineering, Nanyang Technological University, 70 Nanyang Drive 637457, Singapore
[d] Materials Testing & Analysis Center, School of Materials Science and Engineering, Shanghai Jiao Tong University, Shanghai 200240, China

ARTICLE INFO

Article history:
Received 17 December 2010
Received in revised form 4 March 2011
Accepted 8 March 2011
Available online 17 March 2011

Keywords:
TiNi
Equal channel angular extrusion (ECAE)
Aging
R-phase transformation
Ti_3Ni_4

ABSTRACT

Ni-rich TiNi alloys were subjected to the effect of multiple equal channel angular extrusion (ECAE) treatments by B_C path at 500 °C. The characteristics of R phase transformation in aging treatment were dissimilar in the appearance and the temperature range to those counterparts induced by ECAE treatments. The fine lens-like shape Ti_3Ni_4 particles precipitated mainly in the regions of near grain boundaries and on the tangled grain boundaries after ECAE treatments. The effects and mechanisms of aging treatments and ECAE treatments on R phase transformation behaviors and Ti_3Ni_4 precipitates were investigated and discussed.

1. Introduction

As one of the high strain processing ways, equal channel angular extrusion (ECAE) technique has been applied in the production of various ultrafine-grained materials [1–9]. The main ECAE advantage is that imposes a high plastic deformation during pressing without reducing the cross sectional area of working billets. Metals/alloys with the unique combinations of mechanical properties and ultrafine grains can be produced successfully by ECAE technique.

Recently, there were the extensive interests in the ECAE research, and many successful applications have been reported for various metal and alloy materials with ultrafine grains, such as TiNi alloys [10–17], TiAl and TiNb alloys [18,19],Ti [20–22], Mg and Cu alloys [23,24] etc. Among these ultrafine grain materials, Ni-rich TiNi alloys have many applications in engineering and medical fields for their superior properties, such as the shape memory effect (SME) and the pseudoelasticity (PE) [11,25]. The SME and PE properties, which related to martensite phase transformation, were extensively studied in scientific and technological fields [26]. It is well known that Ni-rich TiNi alloys exist three different phases, the B2 parent phase, the B19′ phase and the R phase [27,28]. Three phase transformations can happen possible, which correspond to B2 ↔ B19′ transformation, B2 ↔ R transformation and R ↔ B19′ transformation, respectively. Therefore, different combinations of these phase transformations can be observed under various technological processes [28].

R transformation can be introduced by different methods such as annealing after cold working [29], adding Al or Fe elements in TiNi alloys [30,31]. For Ni-rich TiNi alloys, both aging treatment [32,33] and ECAE treatments [13,14] could lead to the R phase transformation. To date, the mechanism of R phase transformation in Ni-rich TiNi alloys with the aging treatment and the following multiple ECAE treatments are seldom studied systematically. It is still inconclusive whether R transformation in ECAE treatments is induced by ECAE or the aging treatment on TiNi billets before ECAE. In this study, the R phase transformation behaviors of Ni-rich TiNi alloys after aging treatment and subsequent multiple ECAE treatments at warm 500 °C by B_C path are investigated. The reasons and differences of the special R phase transformation behaviors and Ti_3Ni_4 precipitates of positions and appearances with different ECAE treatments are also discussed. This investigation will be helpful for better understanding the R phase transformation behaviors of Ni-rich TiNi alloys after aging and ECAE treatments.

2. Experimental details

The initially hot forged Ni-rich Ti–50.9 at.% Ni alloy (nominal composition) rods with an initial average grain size of ~70 μm were annealed at 850 °C for 1 h (Fig. 3a), and then quenched into water quickly (solution treatment). The inner contact angle (Φ) and the arc of curvature (Ψ) at the outer point of contact between channels of

* Corresponding author. Tel.: +86 21 5474 2608.
E-mail addresses: zxn100@gmail.com (X. Zhang), cyxie@sjtu.edu.cn (C. Xie).

0925-8388/$ – see front matter © 2011 Elsevier B.V. All rights reserved.
doi:10.1016/j.jallcom.2011.03.062

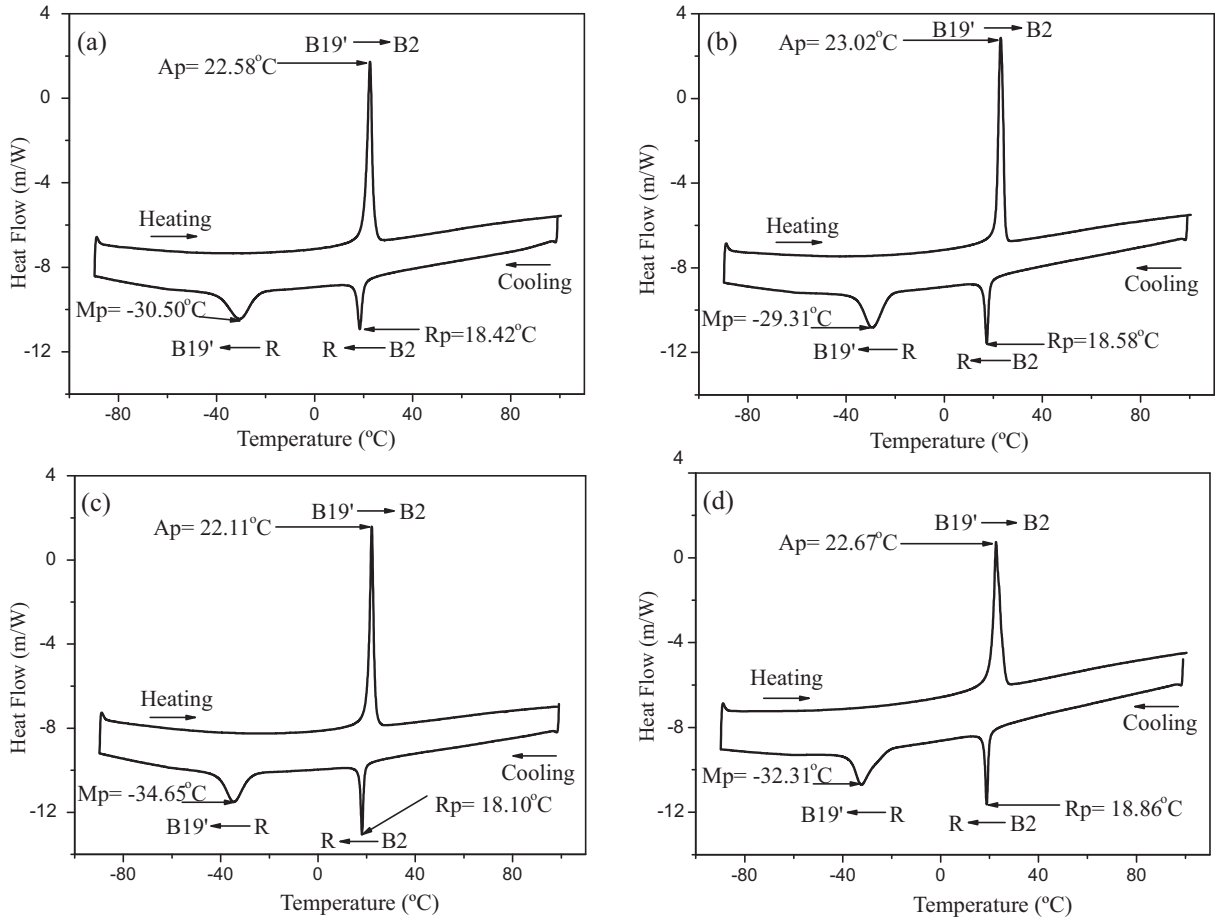

Fig. 1. DSC curves of Ti–50.9 at.% Ni alloy with the aging treatment at 500 °C for 20 min before ECAE treatments at 500 °C by B_C path: (a) first pass; (b) second pass; (c) fourth pass; (d) eighth pass.

the die were both 90°. It was well known that an effective strain of ~1 produced in the single pass of ECAE treatments. The hard-to-deformed Ti–50.9 at.% Ni alloy required a good plasticity to prevent cracking and fracture during ECAE treatments. For this reason, TiNi billets with dimensions of 10 mm × 10 mm × 140 mm need to be processed at 500 °C by B_C path (the billet was rotated by 90° either clockwise or anti-clockwise). And during every ECAE process, the billets were preheated at 500 °C for 20 min. The heated billets surfaces convenient solidified and coated with fluid graphitic lubricant. Graphitic lubricant can minimize the friction, prevent cracking and avoid the surface oxidation of working billets during the ECAE processes. Moreover, the ECAE processes cannot be considered as a thermo-mechanical treatment because the whole duration time of ECAE treatments is less than 10 s under the 8 mm/s constant velocity of ECAE processes.

For the differential scanning calorimeter (DSC) measurements, the metallographic examinations and transmission electron microscopy (TEM) observations, the samples were cut from the longitudinal plane of deformed billets that parallel to the extrusion direction of ECAE. The DSC measurements were carried out with heating and cooling rate 10 °C/min and samples weights of DSC test were between 5 and 10 mg. The range of DSC test temperatures was in −90 to 100 °C by using Diamond DSC machine (PerkinElmer Company of American). The metallographic experiments were performed with Zeiss optical microscope. Samples for TEM observation were prepared by twin jet electro-polishing at −30 °C and with manipulation voltage of 30 V. The twin jet solution was H_2SO_4 and CH_3OH mixture with a volume ratio of 1:4. TEM experiments were conducted on the JEM-2100F (JEOL) with an accelerating voltage of 200 kV.

3. Results

3.1. DSC analyses

R phase transformation behaviors of Ti–50.9 at.% Ni alloy with aging treatment at 500 °C for 20 min and different ECAE treatments were analyzed by DSC measurements, as shown in Figs. 1 and 2, respectively. The phase transformation temperatures of the martensite, R and austenite phase start (Ms, Rs, As), peak (Mp, Rp, Ap) and finish (Mf, Rf, Af) temperature of Ti–50.9 at.% Ni alloy with aging treatment and different ECAE passes were listed in Table 1.

When the specimen was cooled from 100 °C down to −90 °C, two exothermic peaks appeared obviously, which corresponded to from the B2 → R phase and then from the R → B19′ martensite phase transformation. The curves of B2 → R phase transformation of aging treatment were very sharp and clear, as shown in Fig. 1. It indicated that R phase transformation occurred in a very narrow temperature range. However, B2 → R phase transformation of ECAE treatments occurred in a wider temperature extent, and these broad and smooth curves were not very clear peaks (Fig. 2). Additionally, only R phase transformation was observed even the specimen was cooled till −150 °C after the first ECAE pass (Fig. 2a).

When the specimen was heated from −90 °C up to 100 °C, only one endothermic peak appeared. It showed that the reverse B19′ → R phase transformation and the subsequent reverse R → B2 martensite transformation overlapped together [34]. The very clear and apparent DSC curves of aging treatment also revealed the reverse transformation in a narrow temperature range (Fig. 1). However, the broad reverse transformation curves of ECAE treatments indicated that it occurred in a wider temperature range (Fig. 2). Moreover, the Mp, Rp and Ap of aging treatments were stable relatively (Table 1), and no obvious changes were happened after the different ECAE treatments (Fig. 1). However, the Mp and Ap after ECAE have a clear change along with the number of ECAE treatment increases, which are inconsistent with those of aging treatments.

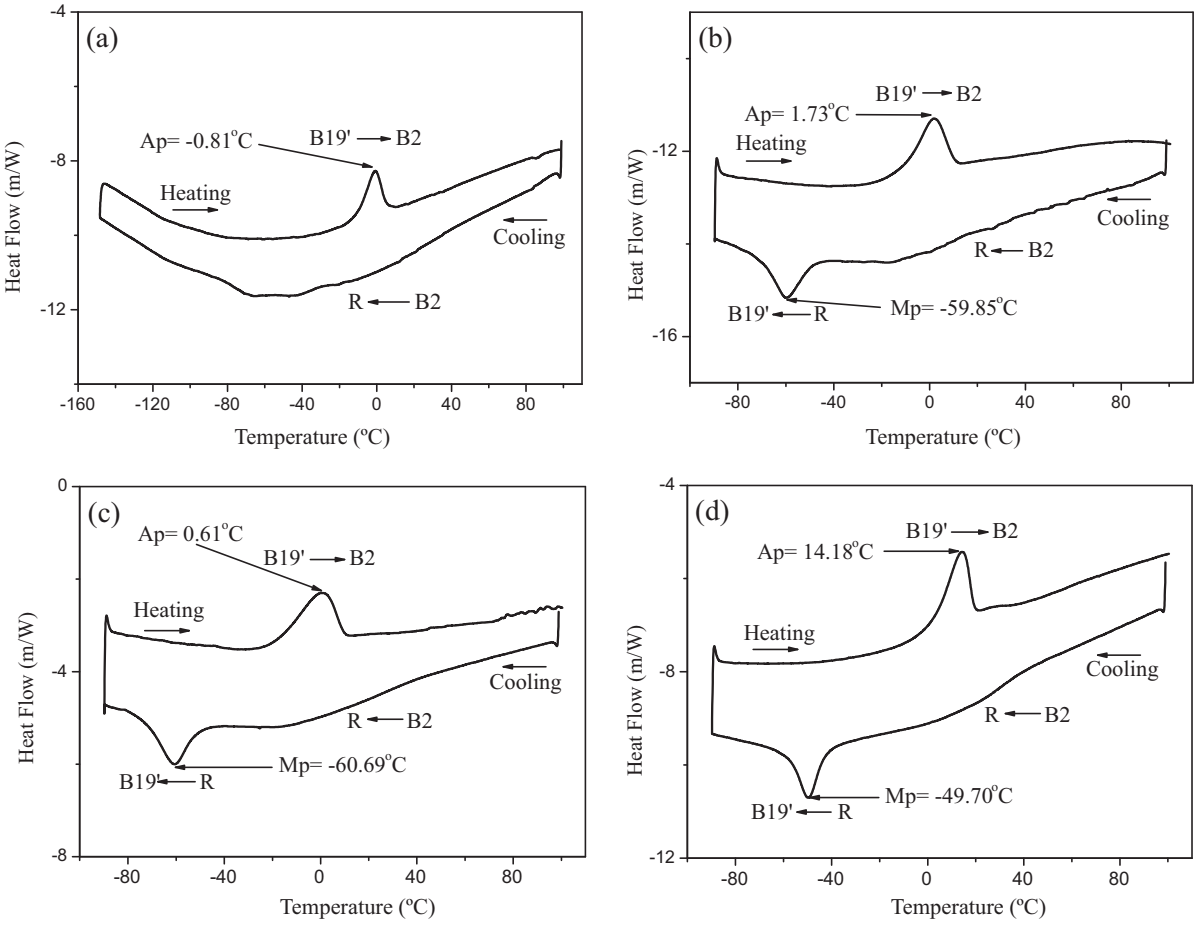

Fig. 2. DSC curves of Ti–50.9 at.% Ni alloy after ECAE treatments at 500 °C by B_C path: (a) first pass; (b) second pass; (c) fourth pass; (d) eighth pass.

3.2. TEM and SAED observations of Ti_3Ni_4 precipitates

The detailed information of Ti_3Ni_4 precipitates including precipitation regions and particles morphologies after ECAE treatments were studied by TEM technique and the corresponding selected area electron diffraction (SAED) patterns.

Ti_3Ni_4 precipitates keep the co-exist relationships with the matrix. The $1/7\langle 123\rangle_{B2}$ super-lattice spots can be observed in SAED along the $<321>_{B2}$ reciprocal direction of the B2 parent phase [35]. As the most important evidence of Ti_3Ni_4 precipitates, the $1/7\langle 123\rangle_{B2}$ super-lattice spots confirm that Ti_3Ni_4 particles existed in the corresponding regions.

The sample obtained after the eighth pass ECAE has a finer submicron grains with an average grain size of about 300–400 nm (Fig. 3b). Fig. 3c and d is the SAED patterns which corresponded to the selected area (marked A and B region in Fig. 3b, respectively). The $1/3\langle 111\rangle_{B2}$ super-lattice spots (marked with some white circles), accompanying with $1/7\langle 123\rangle_{B2}$ super-lattice spots (marked with some white squares bunched by a white line) of the eighth pass ECAE sample also could be observed in the Fig. 3c. However, only the $1/3\langle 111\rangle_{B2}$ super-lattice spots can be observed in the Fig. 3d, the $1/7\langle 123\rangle_{B2}$ super-lattice spots were not observed in this region. It revealed that there was no Ti_3Ni_4 precipitates in the B area. Furthermore, there was R phase transformation formed in both A and B regions but Ti_3Ni_4 precipitates were formed mainly in the A region of near grain boundaries and on the tangled grain boundaries after ECAE treatments [13,28,36]. Based on the inhomogeneous distribution of Ti_3Ni_4 precipitates from TEM and SAED analyses of Fig. 3, the matrix was divided into two specifically distinctive regions. For one part, Ti_3Ni_4 precipitates concentrated on the regions of near grain

Table 1
Phase transformation temperature of Ti–50.9 at.% Ni alloy with the aging treatment at 500 °C for 20 min and after ECAE treatments at 500 °C by B_C path.

Procedures (aging treatment)	Temperature (°C)								
	Ms	Mp	Mf	Rs	Rp	Rf	As	Ap	Af
First ECAE	−23.07	(30.50	(51.08	20.15	18.42	16.50	20.43	22.58	24.11
Second ECAE	(22.26	(29.31	(35.77	17.29	18.58	15.90	21.17	23.02	24.84
Fourth ECAE	(27.54	(34.65	(52.13	19.17	18.10	16.98	20.54	22.11	23.44
Eighth ECAE	(24.51	(32.31	(37.63	19.93	18.86	17.59	20.88	22.67	25.69
(ECAE treatment)									
First ECAE	–	–	–	–	–	–	(9.53	(0.81	17.44
Second ECAE	(50.35	(59.85	(78.33	–	–	–	(10.43	1.73	18.66
Fourth ECAE	(49.55	(60.69	(80.58	–	–	–	(16.93	0.61	14.03
Eighth ECAE	(41.85	(49.70	(68.93	–	–	–	3.36	14.18	19.71

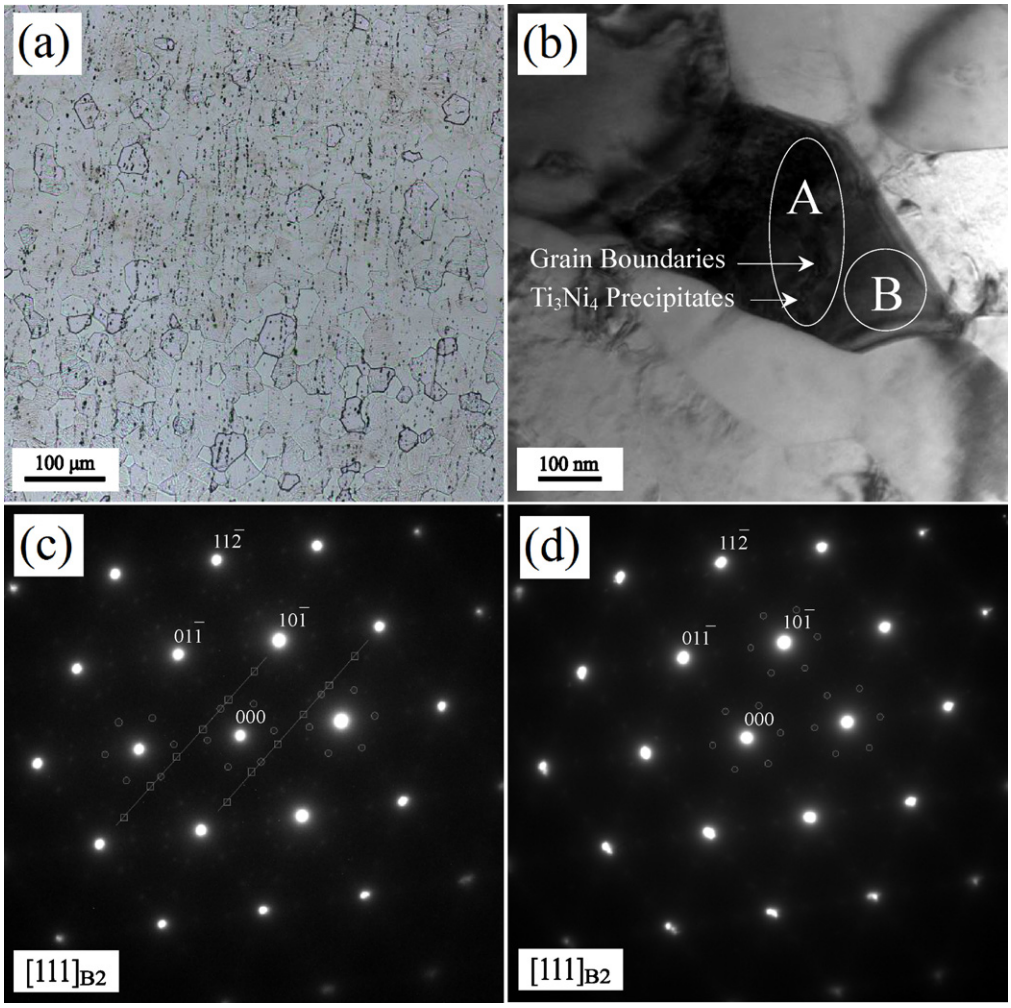

Fig. 3. Microstructures of Ti–50.9 at.% Ni alloy: (a) solution treatment; TEM and SAED patterns with a beam direction parallel to $[1\,1\,1]_{B2}$ of Ti–50.9 at.% Ni alloy after the eighth pass ECAE at 500 °C by B_C path: (b) bright field images of the eighth pass, identifying Ti_3Ni_4 precipitates location; (c) SAED pattern of A regain in Fig. 3b; (d) SAED pattern of B regain in Fig. 3b.

boundaries and on the tangled grain boundaries. For another, there have the relatively free Ti_3Ni_4 precipitates in the interior region of grains.

The detailed information of Ti_3Ni_4 particles morphologies are further studied by SAED and TEM techniques (Fig. 4). The SAED pattern of the sixth pass ECAE treatments shown in Fig. 4a corresponded to beam direction parallel to $[1\,1\,1]_{B2}$. As mentioned before, the $1/3\langle 111\rangle_{B2}$ super-lattice spots and $1/7\langle 123\rangle_{B2}$ super-lattice spots of the sixth pass ECAE sample could be observed in the SAED pattern. Fig. 4b was the TME bright field image of Ti_3Ni_4 precipitates characterized by $1/7\langle 123\rangle_{B2}$ super-lattice spots and Fig. 4c was the dark field image corresponded to Fig. 4b. The homogeneous precipitated Ti_3Ni_4 particles with the lens-like shape was observed in the regions of near grain boundaries and on the tangled grain boundaries (Fig. 4b) and they distributed in size of about 20–30 nm. From the TEM dark field image (Fig. 4c), Ti_3Ni_4 precipitates could be easily observed in these regions.

4. Discussion

Aging treatments and ECAE treatments would result in R phase transformation. However, it is still uncertain whether R transformation in ECAE treatments is induced by ECAE itself or the billets treated by aging treatment before ECAE treatments. The characteristics of R phase transformation in aging treatment were dissimilar in the appearance and the temperature range to those counterparts induced by ECAE treatment due to the essential difference between mechanisms of the two R phase transformations.

For Ni-rich TiNi alloys after aging treatment, the sharper and clear B2 → R phase transformation curves caused in aging treatment can be seen in a narrower temperature range. Furthermore, the Mp, Rp and Ap were no obvious changes happened along with the ECAE treatments (Fig. 1). These phenomena would be attributed to the fine and dense lens-like shape Ti_3Ni_4 precipitates formed by aging treatment. The Ti_3Ni_4 precipitates could act as the pinning sites against the movement of dislocations [37], and create energy barrier for martensite nucleation, which could make R phase transformation in a lower energy alternative. It is agreement with the previous studies on the mechanism of the separation of martensite and R phase transformation. Nishida and Wayman thought that the R phase transformation was induced by the appearance of the homogeneous Ti_3Ni_4 particles with fine lens-like shape after aging treatment [38]. Miyazaki considered the Ti_3Ni_4 precipitates suppressed the martensite phase transformation and resulted in the decreased Ms [39]. Kim reported that the formation of fine and coherent Ti_3Ni_4 precipitates could affect the transformation behavior of the matrix through change in matrix composition and creation of local stress fields [28]. Therefore, the sharp and distinct

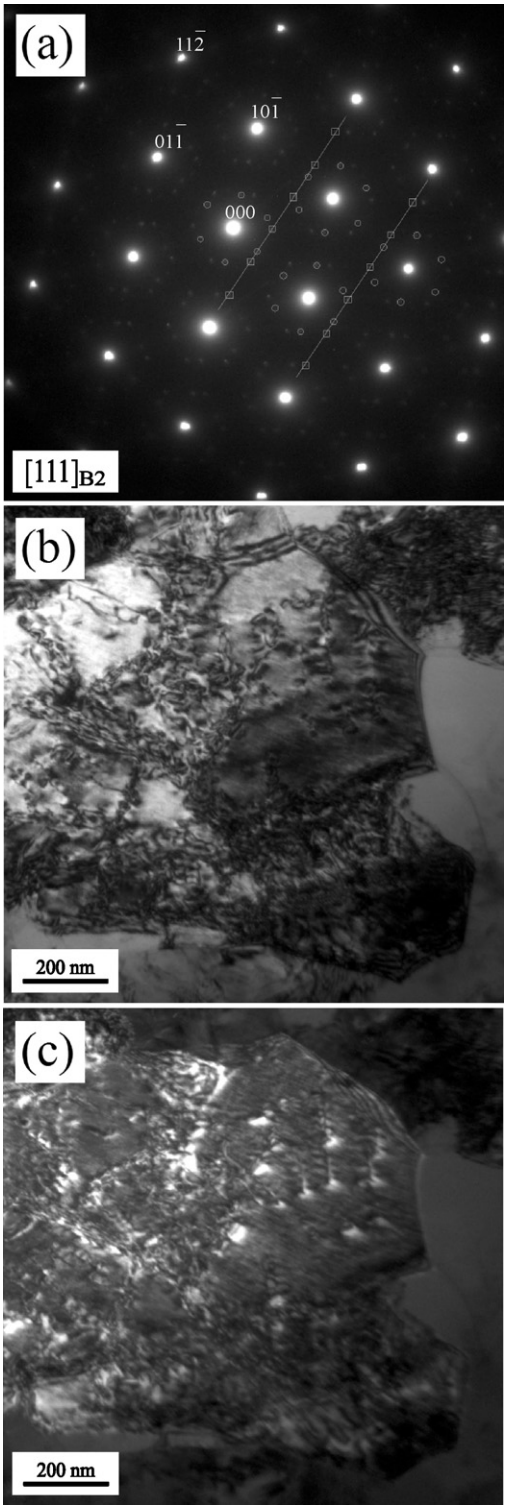

Fig. 4. SAED pattern with a beam direction parallel to $[1\,1\,1]_{B2}$ and TEM images of Ti–50.9 at.% Ni alloy after the sixth pass ECAE at 500 °C by B_C path: (a) SAED pattern, identifying Ti_3Ni_4 precipitates; (b) TEM bright field image; (c) TEM dark field image corresponding to Fig. 4b.

B2 → R phase transformation was induced by Ti_3Ni_4 precipitates of the aging treatment at first, and then coexisted with the subsequent martensite transformations.

However, the B2 → R phase transformation in ECAE treatments appeared in a wider temperature range, and the curves were neither distinctness nor sharp (Fig. 2). In addition, Mp decreased sharply at the beginning of the previous second and fourth ECAE treatments which could be resulted from the effects of deformation suppression on phase transformation to the low temperature [35]. Afterwards the dropped Mp increased along with the eighth ECAE treatments (Table 1), it may be attributed to the precipitations of Ti_3Ni_4 particles. Ti_3Ni_4 precipitates induced by aging treatment did not remelt into the matrix totally after ECAE treatments. From the SAED patterns, the $1/7\langle 123\rangle_{B2}$ super-lattice spots of Ti_3Ni_4 particles can also be observed (Figs. 3c and 4a). From the Figs. 3b and 4b, Ti_3Ni_4 precipitates can be observed in the regions of grain boundaries. These results showed that existence a complex structure containing dislocations and grain boundaries decorated with Ti_3Ni_4 precipitates after the ECAE treatments. Ti_3Ni_4 particles have obvious results on the subsequent martensite transformations. As well known, the precipitation of Ti_3Ni_4 decreased the Ni content in the matrix, which could lead to the increase of the temperature of the martensite phase transformation after the ECAE treatments [40]. The B2 → B19′ transformation was hampered because these diffuse Ti_3Ni_4 particles presented in the matrix would require more additional energy expenditure owing to a higher elastic energy of the system. By contrast, these dispersed Ti_3Ni_4 particles would serve as the nucleation sites of the R phase transformation due to the crystal lattices are similar, the presence of Ti_3Ni_4 in the B2 matrix favor a B2 → R transformation (Fig. 2) [41]. The martensite transformation was occurred the sequence B2 → R → B19′ in nanostructured TiNi based alloys or only a single B2 → R transition could be observed in the amorphous nanocrystalline alloys with the ECAE [13,14].

It was obvious that the broad and smooth B2 → R phase transformation was originated from the introduction of grain refinement and energy accumulation after ECAE treatments. ECAE has the advantages in achieving the bulk materials with the uniform ultrafine grains. In this study, the coarse grain size of Ti–50.9 at% Ni alloy decreased apparently from∼70 μm down to 300–400 nm range after the eighth ECAE pass (Fig. 3a and b), and thus the volume fraction of the grain boundaries increased relatively. All this could be attributed to the continuous dynamic recovery/recrystallization during ECAE treatments. The refined submicron grains and microstructures were also shown to notably change the thermomechanical properties of the present Ti–50.9 at% Ni alloy [42]. These geometrical constraints including the submicron grains and the high density grain boundaries would lead to the transformation barrier and the martensite morphology in the TiNi alloys with ultrafine grains. They also could bring about the change of the thermal stability and martensite transformation path [43]. And thus the reducing of phase transformation temperatures was happened and the broad R phase transformation in deformed Ni-rich TiNi alloys was observed in this present ECAE study.

Additionally, the B2 → B19′ transformation is difficult directly because the only single phase transformation requirement more energy (i.e., reduction in the transformation temperature) in the ECAE treatments. However, multiple phase fronts would nucleate in the transformation from B2 to B19′ through the intermediate R phase transformation, B2 → R → B19′, which need less energy. High density dislocations and grain boundaries not only acted as the media of the nucleation of R phase transformation, which made the R phase formation in a lower energy alternative [44,45]; but also resulted in residual stresses in these regions, which favored the subsequent R transformation in these regions. Therefore, the broad and smooth R phase transformation curves should be induced by ECAE treatment rather than by the aging treatment before ECAE.

5. Conclusions

In this study, the effects of warm temperature ECAE treatments and aging treatment on R phase transformation behaviors and

Ti_3Ni_4 precipitates of Ni-rich TiNi alloys after ECAE were investigated. The following results were obtained:

1. According to DSC observation, R phase transformation could be induced by the aging treatments and ECAE treatments, but their appearance and temperature range were different. The curves of B2 → R phase transformations of aging treatment were very sharp and clear and no obvious changes along with ECAE treatments. However, the B2 → R phase transformation occurred within a wider temperature range and has distinct changes with the increase of ECAE treatments.
2. Ti_3Ni_4 precipitates can be as the main reason of R phase transformation in aging treatment because the internal stress fields can be introduced by the Ti_3Ni_4 precipitates. Ti_3Ni_4 precipitates did not remelt into the matrix totally and still stay in the B2 parent phase during ECAE treatments. From the SAED patterns after ECAE treatments, the $1/7\langle 123\rangle_{B2}$ super-lattice spots of Ti_3Ni_4 particles can be observed. According to TEM observations, Ti_3Ni_4 particles precipitated mainly in the regions of grain boundaries after ECAE treatments.
3. ECAE technique has the advantages in achieving the bulk materials with the refined microstructure such as the ultrafine grains, high density dislocations and the increased volume fraction of the grain boundaries. B2 → R phase transformation in ECAE treatments could be attributed to these refined microstructures and energy accumulation that produced in ECAE treatments. High density dislocations and grain boundaries could act as the media of the nucleation of R phase and thus make the R phase formation in a lower energy alternative.

Acknowledgement

Our research was supported by National Science Fund of China (grant no. A50671067 and 51001072).

References

[1] Q. Chen, S. Luo, Z. Zhao, J. Alloys Compd. 477 (2009) 726–731.
[2] S. Biswas, S.S. Dhinwal, S. Suwas, Acta Mater. 58 (2010) 3247–3261.
[3] O.V. Mishin, J.R. Bowen, S. Lathabai, Scripta Mater. 63 (2010) 20–23.
[4] W.N. Tang, R.S. Chen, E.H. Han, J. Alloys Compd. 477 (2009) 636–643.
[5] Y. Huang, J.D. Robson, P.B. Prangnell, Acta Mater. 58 (2010) 1643–1657.
[6] G.B. Hamu, D. Eliezer, L. Wagner, J. Alloys Compd. 468 (2009) 222–229.
[7] N. Tabatabaei, A.K. Taheri, M. Vaseghi, J. Alloys Compd. 502 (2010) 59–62.
[8] A. Hasani, L.S. Tóth, Scripta Mater. 61 (2009) 24–27.
[9] S. Poortmans, L. Duchêne, A.M. Habraken, B. Verlinden, Acta Mater. 57 (2009) 1821–1830.
[10] B. Kockar, K.C. Atli, J. Ma, M. Haouaoui, I. Karaman, M. Nagasako, R. Kainuma, Acta Mater. 58 (2010) 6411–6420.
[11] R. Lahoz, J.A. Puértolas, J. Alloys Compd. 381 (2004) 130–136.
[12] R. Kocich, I. Szurman, M. Kursa, J, Fiala, Mater. Sci. Eng. A. 512 (2009) 100–104.
[13] V.G. Pushin, V.V. Stolyarov, R.Z. Valiev, N.I. Kourov, N.N. Kuranova, E.A. Prokofiev, L.I. Yurchenko, Ann. Chim. Sci. Mater. 27 (2002) 77–88.
[14] V.G. Pushin, V.V. Stolyarov, R.Z. Valiev, T.C. Lowe, Y.T. Zhu, Mater. Sci. Eng. A 410–411 (2005) 386–389.
[15] X. Zhang, J. Song, C. Huang, B. Xia, B. Chen, X. Sun, C. Xie, J. Alloys Compd. 509 (2011) 3006–3012.
[16] K.C. Atli, I. Karaman, R.D. Noebe, H.J. Maier, Scripta Mater. 64 (2011) 315–318.
[17] R. Kocich, M. Kursa, I. Szurman, A. Dlouhy, J. Alloys Compd. 509 (2011) 2716–2722.
[18] K. Morsi, S. Goyal, J. Alloys Compd. 429 (2007) L1–L4.
[19] J. Ma, I. Karaman, H.J. Maier, Y.I. Chumlyakov, Acta Mater. 58 (2010) 2216–2224.
[20] T. Niendorf, D. Canadinc, H.J. Maier, I. Karaman, Scripta Mater. 60 (2009) 344–347.
[21] Y.J. Chen, Y.J. Li, J.C. Walmsley, S. Dumoulin, S.S. Gireesh, S. Armada, P.C. Skaret, H.J. Roven, Scripta Mater. 64 (2011) 904–907.
[22] Y.J. Chen, Y.J. Li, J.C. Walmsley, S. Dumoulin, P.C. Skaret, H.J. Roven, Mater. Sci. Eng. A 527 (2010) 789–796.
[23] J. Jiang, Y. Wang, J. Qu, Z. Du, Y. Sun, S. Luo, J. Alloys Compd. 497 (2010) 62–67.
[24] T. Grosdidier, D. Goran, G. Ji, N. Llorca, J. Alloys Compd. 504 (2010) S456–S459.
[25] X. Xu, X. Lin, M. Yang, J. Chen, W. Huang, J. Alloys Compd. 480 (2009) 782–787.
[26] I. karaman, H.E. Karaca, H.J. Maier, Z.P. Luo, Metall. Mater. Trans. A 34 (2003) 2527–2539.
[27] T. Waitz, V. Kazykhanov, H.P. Karnthaler, Acta Mater. 52 (2004) 137–147.
[28] J.I. Kim, Y. Liu, S. Miyazaki, Acta Mater. 52 (2004) 487–499.
[29] H. Morawiec, D. Stró, T. Goryczka, D. Chrobak, Scripta Mater. 35 (1996) 485–490.
[30] C.M. Hwang, C.W. Wayman, Scripta Metall. 17 (1983) 1449–1453.
[31] C.M. Hwang, M. Meichle, M.B. Salamon, C.M. Wayman, Philos. Mag. A 47 (1983) 9–30.
[32] S. Miyazaki, K. Otsuka, Met. Trans. A (1986) 53–63, 17A.
[33] Y. Liu, X. Chen, P.G. McCormick, J. Mater. Sci. 32 (1997) 5979–5984.
[34] G. Fan, W. Chen, S. Yang, J. Zhu, X. Ren, K. Otsuka, Acta Mater. 52 (2004) 4351–4362.
[35] S. Miyazaki, Y. Igo, K. Otsuka, Acta Mater. 34 (1986) 2045–2051.
[36] J.K. Allafi, A. Dlouhy, G. Eggeler, Acta Mater. 50 (2002) 4255–4274.
[37] J.I. Kim, S. Miyazaki, Acta Mater. 53 (2005) 4545–4554.
[38] M. Nishida, C.M. Wayman, Metall. 21 (1988) 255–273.
[39] S. Miyazaki, C.M. Wayman, Acta Mater. 36 (1988) 181–192.
[40] M. Nishida, C.M. Wayman, T. Honma, Metall. Trans. A 17 (1986) 1505–1515.
[41] V.I. Zel'dovich, G.A. Sobyanina, V.G. Pushin, Scripta Mater. 37 (1997) 79–84.
[42] B. Kockar, I. Karaman, J.I. Kim, Y.I. Chumlyakov, J. Sharp, C. Yu, Acta Mater. 56 (2008) 3630–3646.
[43] T. Waitz, T. Antretter, F.G. Fischer, N.K. Simha, H.P. Karnthaler, J. Mech. Phys. Solids 55 (2007) 419–444.
[44] C.P. Frick, A.M. Ortega, J. Tyber, A. El. M. Maksound, H.J. Maier, Y. Liu, K. Gall, Mater. Sci. Eng. A 405 (2005) 34–49.
[45] M.C. Carroll, C. Somsen, G. Eggeler, Scripta Mater. 50 (2004) 187–192.